Modeling and Analysis of an Optically-Actuated, Bistable MEMS Device

Vijay Kumar
e-mail: kumar2@purdue.edu

Jeffrey F. Rhoads[1]
e-mail: jfrhoads@purdue.edu

School of Mechanical Engineering,
Birck Nanotechnology Center,
and Ray W. Herrick Laboratories,
Purdue University,
West Lafayette, IN 47907

Bistable microsystems have drawn considerable interest from the MEMS/NEMS research community not only due to their broad applicability in commercial applications, such as switching, but also because of the rich dynamic behavior they commonly exhibit. While a number of prior investigations have studied the dynamics of bistable microsystems, comparatively few works have sought to characterize their transient behavior. The present effort seeks to address this through the modeling and analysis of an optically-actuated, bistable MEMS switch. This work begins with the development of a distributed-parameter representation for the system, which is subsequently reduced to a lumped-mass analog and analyzed through the use of numerical simulation. The influence of various system and excitation parameters, including the applied axial load and optical actuation profile, on the system's transient response is then investigated. Ultimately, the methodologies and results presented herein should provide for a refined predictive design capability for optically-actuated, bistable MEMS devices. [DOI: 10.1115/1.4005080]

1 Introduction

As their name suggests, bistable systems feature two, coexistent stable states. Depending on the system's energy level, a given bistable device can oscillate about one of its two states and decay, switch one or more times between states then decay, or exhibit stochastic behavior, such as stochastic resonance [1,2]. In the mechanical domain, research related to bistable systems stems largely from early investigations of structural buckling and post-buckled dynamics. Recent, yet representative, works include those of Emam [3], which considered the complex, quasi-periodic and chaotic response of post-buckled beams, Chen and Liao [4], which studied the dynamics of a post-buckled beam under the influence of an impact load at the end, and Yabuno and Tsumoto [5], which explored the transient behavior of a buckled beam in the presence of a high-frequency direct excitation. In the context of micro- and nanoscale systems, bistable devices have garnered significant interest not only due to their rich dynamics, but also due to their broad applicability in commercial applications, such as switching and microfluidics (see, for example, Refs. [6–8]). Representative of works in this area are the collective efforts of Saif and collaborators [9–11], which the present work seeks to build upon, the work of Qin [8], which considered the dynamics of an electrothermally-actuated, bistable MEMS device, and, more recently, the works of Krylov and collaborators, which considered the bistable behavior of electrostatically-actuated MEMS structures operating near pull-in and/or snap-in [12,13].

The bistable MEMS device of interest is a long slender beam, clamped at both ends, which is connected to an actuator that provides an axial compressive load (see Fig. 1) [9]. In this system, as the compressive force is increased beyond a critical load the beam buckles (the response bifurcates), yielding two coexistent stable configurations and an intermediate unstable state, which is often analogous to the device's unbuckled configuration. In prior work, Sulfridge and collaborators modeled the static response of this representative microscale system, after it had buckled in the first mode [10,11]. Building upon this, successive efforts by the same research group considered optically-induced switching, realized via the application of an external laser pulse, and the impact of system nonlinearities. These works explained the switching between bistable states through the use of numerical simulations, and their behavioral predictions were subsequently verified experimentally.

Although the dynamics of the bistable system of interest were previously investigated in Ref. [11], the analytical approaches utilized in that work have some limitations. First, the previously developed model is based upon a lumped-mass representation, which itself was based on a previously developed static model. Additionally, the work assumed that the beam buckles only in the first mode of a clamped-clamped beam, which might not always be the case in practical applications where intermediate boundary conditions may be present. In light of these limitations, the objective of this work is to develop a refined model for the system of interest, which can be subsequently used to characterize the bistable device's transient response under various forcing conditions and, ultimately, to efficiently predict switching times. To this end, this work begins with the development of a distributed-parameter model for the bistable system suitable for the analysis of both buckling and post-buckling dynamics. An optical actuation force is then appended to this model and the switching behavior of the device is studied for various optical actuation profiles. The work concludes with a brief summary and an overview of ongoing and future work.

2 System Modeling

The particular bistable system of interest, previously considered in Ref. [11], is shown in Fig. 1. This system consists of a rectangular beam (the line segment between points A and B) with dimensions 1000 $\mu m \times 100\ \mu m \times 5\ \mu m$, which is anchored at both ends and buckled by a compressive force provided by the comb-driven actuator connected at B. The known actuator force contributes to the displacement of both the buckled beam and the actuator springs. The laser source, which provides the transverse actuation (switching) force, is designated by L. For analytical purposes, this system can be simplified to the model depicted in Fig. 2. The modeling procedure is similar to the one followed in Refs. [14,15].

In Fig. 2, $F(s,t)$ represents the transverse external force applied on the beam. This force is used to switch between stable states after the onset of buckling. M represents the mass of the actuator, and P represents the force provided by the actuator. Note that this model neglects the effects of damping on the actuator. If ρ, A, E, I, and l represent the mass density, cross-sectional area, elastic

[1] Corresponding author.

Manuscript received January 11, 2011; final manuscript received September 8, 2011; published online January 6, 2012. Assoc. Editor: D. Dane Quinn.

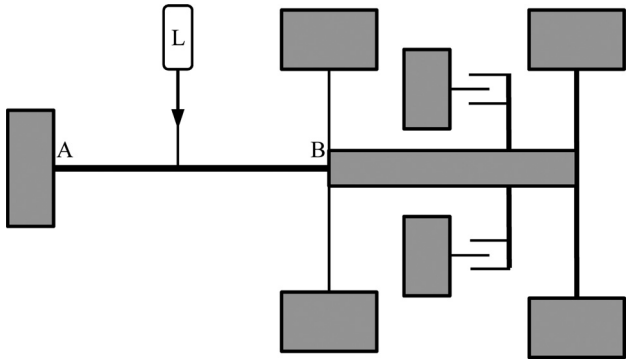

Fig. 1 Schematic diagram of the bistable microsystem of interest

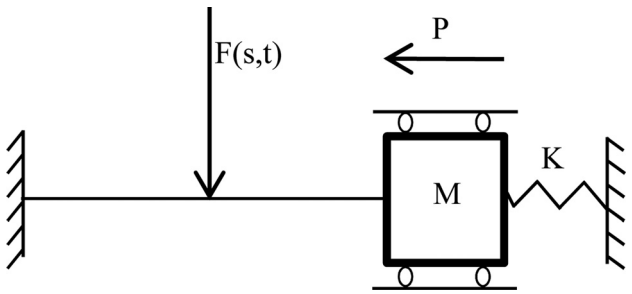

Fig. 2 Diagram of the simplified device representation used for modeling

modulus, area moment of inertia, and length of the beam respectively, and u and w represent the displacements in the longitudinal and transverse directions respectively, the kinetic and the potential energies associated with the beam can be written as

$$T = \frac{1}{2}\int_0^l \rho A\left(\dot{u}^2 + \dot{w}^2\right)\mathrm{d}s$$
$$U = \frac{1}{2}\int_0^l EI(\psi')^2\mathrm{d}s \tag{1}$$

where, $(\dot{\bullet})$ and $(\bullet)'$ represent temporal and spatial derivatives taken with respect to the variables t and arc length variable s respectively, and ψ represents the kinematic constraint relating the transverse and longitudinal deformations to the beam's angular deflection and is given by

$$\tan\psi = \frac{w'}{1+u'} \tag{2}$$

The Lagrangian of the system is defined as

$$L = T - U + \frac{1}{2}\lambda\left[1 - (1+u')^2 - w'^2\right]$$

where λ is a Lagrange multiplier introduced to maintain the inextensibility constraint. The known external load from the actuator, the restoring force in the spring, and the inertia of the actuator is modeled as non-conservative force contributions, according to

$$P_{eff} = -P - Ku(s,t)\delta(s-l) - M\ddot{u}(s,t)\delta(s-l) \tag{3}$$

where, K and M represent the stiffness and the mass of the actuator respectively. Accounting for the damping and the transverse actuation load as non-conservative forces and employing extended Hamilton's principle yields two equations governing the longitudinal and transverse vibrations of the system. Imposing the inextensibility constraint, solving for the Lagrange multiplier in the equation for longitudinal motion, and substituting the result renders the equation of motion governing the transverse vibrations of the system:

$$\begin{aligned}
&\rho A\ddot{w} + C\dot{w} + EIw^{iv} + Pw'' \int_l^s \delta(s-l)\mathrm{d}s + EI(w'')^3 \\
&+ 4EIw'w''w''' + EI(w')^2 w^{iv} + \frac{3}{2}P(w')^2 w'' \int_l^s \delta(s-l)\mathrm{d}s \\
&+ \frac{\rho A}{2}w'' \int_l^s \frac{\partial^2}{\partial t^2}\int_0^s (w')^2\mathrm{d}s\mathrm{d}s + \frac{\rho A}{2}w' \frac{\partial^2}{\partial t^2}\int_0^s (w')^2\mathrm{d}s \\
&- \frac{K}{2}w'' \int_l^s \int_0^s (w')^2\mathrm{d}s\delta(s-l)\mathrm{d}s \\
&- \frac{M}{2}w'' \int_l^s \frac{\partial^2}{\partial t^2}\int_0^s (w')^2\mathrm{d}s\delta(s-l)\mathrm{d}s = F(s,t)
\end{aligned} \tag{4}$$

Equation (4) can be nondimensionalized by scaling the spatial variable with respect to the undeformed length of the beam, the beam displacements with respect to a characteristic length w_0 (for example the beam's thickness), and the time variable with respect to a characteristic period of the system's response, namely,

$$\hat{s} = \frac{s}{l}, \quad \hat{w} = \frac{w}{w_0}, \quad \hat{t} = \frac{t}{T} \tag{5}$$

where

$$T = \sqrt{\frac{\rho A l^4}{EI}}$$

This yields a final distributed parameter model for the system given by

$$\begin{aligned}
&\ddot{\hat{w}} + \hat{c}\dot{\hat{w}} + \hat{w}^{iv} + 4n^2\pi^2\frac{P}{P_{cr}}\hat{w}'' \int_1^{\hat{s}} \delta(\hat{s}-1)\mathrm{d}\hat{s} + \frac{w_0^2}{l^2}(\hat{w}'')^3 \\
&+ 4\frac{w_0^2}{l^2}\hat{w}'\hat{w}''\hat{w}''' + \frac{w_0^2}{l^2}(\hat{w}')^2\hat{w}^{iv} + \frac{3}{2}\frac{w_0^2 P}{EI}(\hat{w}')^2\hat{w}'' \int_1^{\hat{s}} \delta(\hat{s}-1)\mathrm{d}\hat{s} \\
&+ \frac{1}{2}\frac{w_0^2}{l^2}\hat{w}'' \int_1^{\hat{s}} \frac{\partial^2}{\partial\hat{t}^2}\int_0^{\hat{s}} (\hat{w}')^2\mathrm{d}\hat{s}\mathrm{d}\hat{s} + \frac{1}{2}\frac{w_0^2}{l^2}\hat{w}' \frac{\partial^2}{\partial\hat{t}^2}\int_0^{\hat{s}} (\hat{w}')^2\mathrm{d}\hat{s} \\
&- \frac{K}{2}\frac{w_0^2 l}{EI}\hat{w}'' \int_1^{\hat{s}} \int_0^{\hat{s}} (\hat{w}')^2\mathrm{d}\hat{s}\delta(\hat{s}-1)\mathrm{d}\hat{s} \\
&- \frac{M}{2}\frac{w_0^2}{\rho A l^3}\hat{w}'' \int_1^{\hat{s}} \frac{\partial^2}{\partial\hat{t}^2}\int_0^{\hat{s}} (\hat{w}')^2\mathrm{d}\hat{s}\delta(\hat{s}-1)\mathrm{d}\hat{s} = \frac{l^4}{EIw_0}F(\hat{s},\hat{t})
\end{aligned} \tag{6}$$

where

$$\hat{c} = \frac{CT}{\rho A}, \quad P_{cr} = \frac{4n^2\pi^2 EI}{l^2}$$

Note that the critical Eulerian buckling load associated with the system, P_{cr}, can be derived following the procedure outlined in Ref. [16].

The distributed-parameter model developed above can be reduced to a lumped-mass analog by decomposing the displacement variable $\hat{w}$ into its spatial and temporal components according to

$$\hat{w} = z(\hat{t})\Phi(\hat{s})$$

and projecting the result onto a single mode shape. This results in a final governing equation of motion for the system given by

$$m\ddot{z} + c\dot{z} + k_1 z + k_3 z^3 + \alpha_n(z\dot{z}^2 + z^2\ddot{z}) = \eta(\hat{t}) \tag{7}$$

with nondimensional parameters defined as in Table 1.

Table 1 Nondimensional Parameters for the Governing Equation of Motion

$$m = \int_0^1 \Phi^2 \mathrm{d}\hat{s}$$

$$c = \hat{c}\int_0^1 \Phi^2 \mathrm{d}\hat{s}$$

$$k_1 = \int_0^1 \Phi\Phi^{iv}\mathrm{d}\hat{s} + \frac{4n^2\pi^2 P}{P_{cr}}\int_0^1 \Phi\Phi''\int_1^{\hat{s}}\delta(\hat{s}-1)\mathrm{d}\hat{s}\mathrm{d}\hat{s}$$

$$k_3 = \frac{w_0^2}{l^2}\int_0^1 \Phi(\Phi'')^3\mathrm{d}\hat{s} + 4\frac{w_0^2}{l^2}\int_0^1 \Phi\Phi'\Phi''\Phi'''\mathrm{d}\hat{s} + \frac{w_0^2}{l^2}\int_0^1 \Phi(\Phi')^2\Phi^{iv}\mathrm{d}\hat{s} + \frac{3w_0^2}{2}\frac{P}{P_{cr}}4n^2\pi^2\int_0^1 \Phi(\Phi')^2\Phi''\int_1^{\hat{s}}\delta(\hat{s}-1)\mathrm{d}\hat{s}\mathrm{d}\hat{s} - \frac{Kw_0^2 l}{2EI}\int_0^1 \Phi\Phi''\int_0^{\hat{s}}\int_0^1 (\Phi')^2\mathrm{d}\hat{s}\delta(\hat{s}-1)\mathrm{d}\hat{s}\mathrm{d}\hat{s}$$

$$\alpha_n = \frac{w_0^2}{l^2}\int_0^1 \Phi\Phi''\int_1^{\hat{s}}\int_0^{\hat{s}}\Phi'^2\mathrm{d}\hat{s}\mathrm{d}\hat{s}\mathrm{d}\hat{s} + \frac{w_0^2}{l^2}\int_0^1 \Phi\Phi'\int_0^{\hat{s}}\Phi'^2\mathrm{d}\hat{s}\mathrm{d}\hat{s} - \frac{Mw_0^2}{\rho A l^3}\int_0^1 \Phi\Phi''\int_0^{\hat{s}}\int_0^1 (\Phi')^2\mathrm{d}\hat{s}\delta(\hat{s}-1)\mathrm{d}\hat{s}\mathrm{d}\hat{s}$$

$$\eta = \frac{l^4}{EIw_0}\int_0^1 \Phi F(\hat{s},\hat{t})\mathrm{d}\hat{s}$$

The static buckled mode shapes associated with the system of interest (see Fig. 3) can be explicitly obtained by dropping the time-varying terms in Eq. (6) and solving the resulting spatial differential equation:

$$\Phi^{iv} + \hat{P}\Phi'' - \frac{w_0^2 lK}{2EI}\Phi''\int_0^1 (\Phi')^2\mathrm{d}\hat{s} = 0 \tag{8}$$

with

$$\hat{P} = \frac{Pl^2}{EI}$$

and associated boundary conditions given by,

$$\begin{aligned} \Phi = 0 \quad \text{and} \quad \Phi' = 0 \quad \text{at} \quad \hat{s} = 0 \\ \Phi = 0 \quad \text{and} \quad \Phi' = 0 \quad \text{at} \quad \hat{s} = 1 \end{aligned} \tag{9}$$

Given that $\int_0^1 (\Phi')^2\mathrm{d}\hat{s}$ is constant for a particular mode, the general solution of Eq. (8) can be expressed as,

$$\Phi = c_1 + c_2 s + c_3\cos(\sqrt{\lambda}s) + c_4\sin(\sqrt{\lambda}s) \tag{10}$$

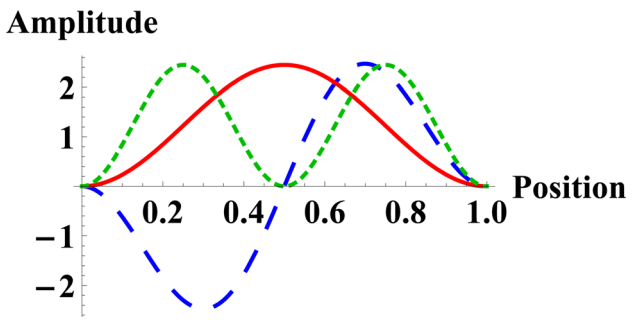

Fig. 3 Static buckled mode shapes associated with the system of interest. The red (solid) and green (dotted) lines represent the first and second symmetric modes of the system, and the blue (dashed) line represent the first antisymmetric mode of the system.

where

$$\lambda = \hat{P} - \left(\frac{w_0^2 lK}{2EI}\right)Q$$

and $Q = \int_0^1 (\Phi')^2\mathrm{d}\hat{s}$. Substituting Eq. (10) into Eq. (9) and solving the resulting algebraic equations yields the following characteristic equation:

$$2 - 2\cos\sqrt{\lambda} - \sqrt{\lambda}\sin\sqrt{\lambda} = 0 \tag{11}$$

The solutions of Eq. (11) can be classified into two varieties: those corresponding to symmetric modes and those corresponding to asymmetric modes. These modes appear in alternating pairs with increasing λ. The first two solutions corresponding to asymmetric modes are 80.763 and 238:718, respectively. Using these values of λ, the asymmetric mode shape of the system can be evaluated to be

$$\Phi = b_n\left[\frac{\frac{1}{\sqrt{\lambda}}\sin\sqrt{\lambda} - 1}{1 - \cos\sqrt{\lambda}} + s - \left(\frac{\frac{1}{\sqrt{\lambda}}\sin\sqrt{\lambda} - 1}{1 - \cos\sqrt{\lambda}}\right)\cos\sqrt{\lambda}s - \frac{1}{\sqrt{\lambda}}\sin\sqrt{\lambda}s\right] \tag{12}$$

The coefficients b_n can be explicitly evaluated by using the relationship between λ and Q. For symmetric modes, the values of λ are given by $4n^2\pi^2$, where n is an integer. The corresponding symmetric mode shapes are given by

$$\Phi = \frac{1}{2}b_n[1 - \cos(2n\pi s)] \tag{13}$$

where,

$$b_n = \sqrt{\frac{\hat{P} - 4n^2\pi^2}{\frac{1}{2}\left(\frac{w_0^2 lK}{2EI}\right)n^2\pi^2}}$$

Using these equations, the nondimensional parameters associated with the equation of motion can be explicitly evaluated.

The optical actuation force utilized for switching can be modeled using the theories of classical physics. Maxwell predicted that since light possesses momentum, if light is absorbed or reflected by a body, it exerts a pressure on that body. The resulting force is given by Ref. [10]

$$F = \frac{2W}{c} \tag{14}$$

where W is the power of the (laser) source and c is the speed of light. In the context of MEMS, the scaling of an optical actuation force compares well with that of electrostatic forces. However, using a laser pulse as an actuation force does have some limitations, namely, diffraction, collimation, and local heating [10]. For example, no surface is completely reflective and hence, some amount of energy must be absorbed into a system being excited by an external laser pulse. This causes some degree of local heating. Previous works have considered the use of local heating as an actuation (switching) mechanism (see, for example, Refs. [17,18]). In this work, following Sulfridge et al. [19], the pressure exerted by the incident radiation is considered to be quite significant compared to heating effects, and therefore, radiation pressure is assumed to be the only external force acting on the device that is capable of inducing switching.

3 Analysis

The static post-buckled behavior of the system can be studied by neglecting the time derivatives and forcing in Eq. (7). Analysis of the resulting equation, after projection onto the first symmetric

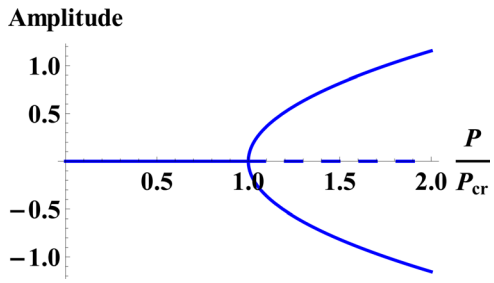

Fig. 4 Static behavior of the beam at its first symmetric buckling mode. The beam shows a supercritical pitchfork behavior with the zero solution becoming unstable and two additional stable solutions arising as the axial load is increased beyond the critical Eulerian load. Solid lines represent stable solutions, while dashed lines represent the unstable solution of the system.

buckling mode, reveals classical supercritical pitchfork behavior (see Fig. 4). Thus, static buckling behavior can be sufficiently captured by the model.

Though multi-mode approximations are commonly used to describe the dynamic behavior of buckled systems, in the case of a buckled beam with a transverse actuation force applied at the midpoint, the system's higher modes do not contribute appreciably to the accuracy of the solution [20]. Accordingly, a single symmetric mode approximation is used to investigate the post-buckling dynamics of the bistable system of interest. The dynamics of this system largely depend on how large the applied axial load is in comparison to the critical buckling load associated with the system. In order to study this effect, the phase plane associated with the system for two different initial conditions and two different axial loads is considered. Figure 5(*a*) shows the phase plane for the system when the axial load is 1% higher than the critical buckling load, and Fig. 5(*b*) shows the phase plane for the system when the axial load is 5% higher than the critical buckling load of the beam. It can be seen from these phase planes that there are two stable solutions (spiral points) corresponding to the extreme

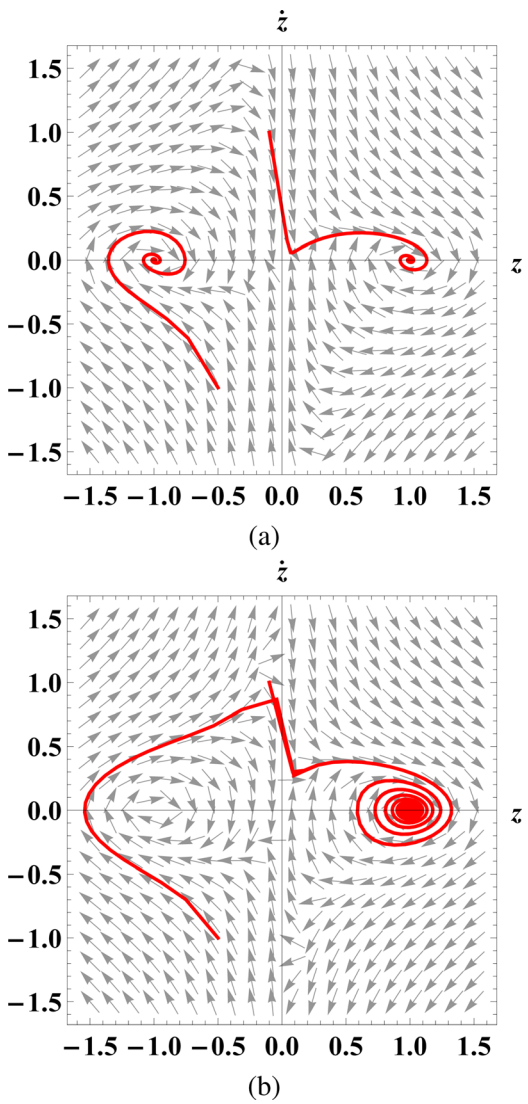

Fig. 5 Phase plane for the buckled beam in its first symmetric buckling mode, when the load is (*a*) 1% and (*b*) 5% higher than the critical load of the system. There are two stable spirals at (±1,0) and a saddle point at (0,0). Note that the following nominal values are used for all simulations unless otherwise stated. The mass of the actuator (M) is about 10 times the mass of the beam, K = 1000 and c = 0.1.

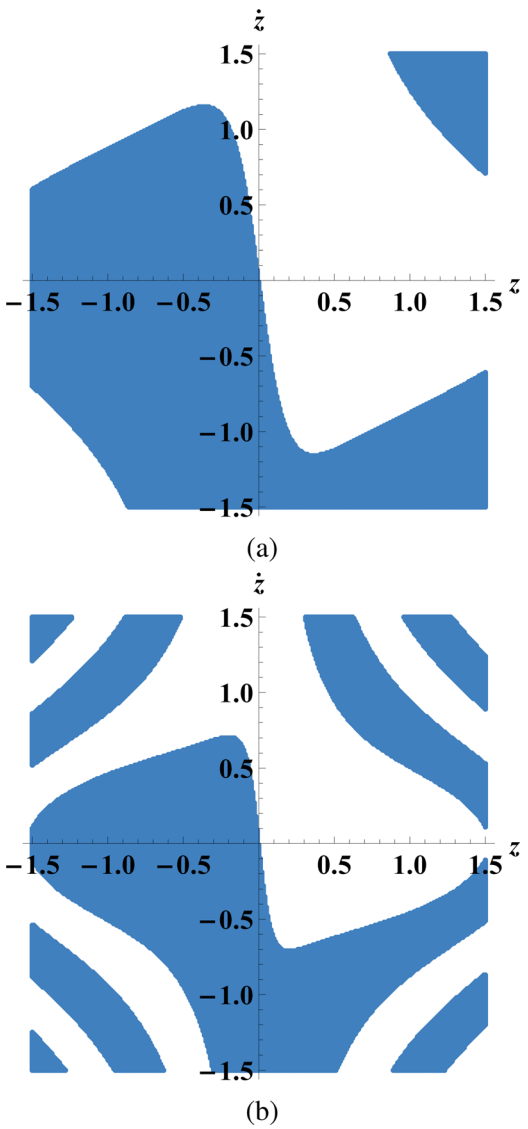

Fig. 6 Basins of attraction for the two stable configurations of the system buckled in its first mode when the load is (*a*) 1% and (*b*) 5% greater than the critical load. Note that the blue areas represent the basin of attraction for the stable point (-1,0) and the white area represents the basin of attraction for the stable point (1,0).

positions of the beam and one unstable solution (saddle point) corresponding to the unbuckled configuration. A small perturbation in the operating condition of the beam gives rise to oscillations in the system. Due to the presence of damping, in most situations the system settles down onto one of its stable states. Of particular note is the fact that for the same initial condition, depending on the value of the applied axial load (and hence, the maximum displacement of the beam), the response of the system may be fundamentally different.

To study the effect of small perturbations on the system, the basins of attraction associated with the system have been plotted. Figure 6(*a*) shows the basins of attraction for the case where the axial load is 1% higher than the critical load, and Fig. 6(*b*) shows the same for the case where the buckling load is 5% higher than the critical load. It can be seen that the basins of attraction quantitatively change as the compressive load is increased, with each of the respective lobes changing in size but largely maintaining shape.

To examine the effects of viscous damping, the basins of attraction have been plotted (Fig. 7) for the cases where the axial load is 1% higher than the critical load, and the viscous damping coefficient is 10% of the value used in Fig. 5. It can be seen that viscous damping plays a significant role in determining the size of the basin lobes, which, in turn, determines the amount of energy required for the beam to switch from one stable state to another. As expected, at lower damping levels, less energy is needed to switch the system to the other stable state. It is also worthwhile noting that as the initial conditions move farther from the stable state, the system has a higher probability of exhibiting multiple transitions or bouncing between the stable states. Finally, it should also be noted that for any given forcing amplitude or pulse time, there exists a threshold value of damping above which the system does not exhibit multiple transitions. By adopting a procedure similar to that utilized above, the effects of the mass of the actuator on the basins of attraction can also be studied. Figure 8 shows the basins of attraction of the system for the cases where the buckling load is 1% and 5% higher than the critical load and the mass of the actuator is 1.5 times the nominal value used in Fig. 5. As evident, as the mass of the actuator increases, the shape of the lobes significantly deform, which in turn, changes the minimum actuation energy required and, thus, the minimum actuation time required for switching.

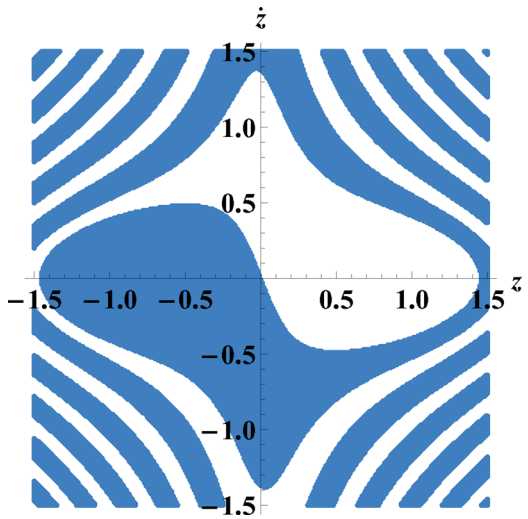

Fig. 7 Basins of attraction for the two stable configurations of the system buckled in its first mode when the load is 1% greater than the critical load. c = 0.01 and all other parameters are as in Fig. 5. Note that the blue areas represent the basin of attraction for the stable point (−1,0) and the white area represents the basin of attraction for the stable point (1,0).

Using the above results as a benchmark, the transient (switching) behavior of the system can be investigated through the use of forward-time numerical simulation. For present purposes, the beam is initially considered to be in the stable position (-1,0) and to have an axial compressive load 0.5% higher than the critical load for buckling. The viscous damping is assumed to be the same as in Figs. 5 and 6. A simple pulse is then applied. Figure 9 shows the response of the system for a simple laser pulse (5 mW power) applied for 0.4 ms and 0.8 ms, respectively. As evident, the system switches to the other stable state for the pulse of 0.8 ms, but not for the pulse of 0.4 ms. Similarly, Fig. 10 shows the response of the system when a half-sine wave shaped laser pulse is applied for 0.4 ms and 0.8 ms respectively. Here, as with the simple pulse, the system switches from one stable state to the other for a pulse 0.8 ms in duration, but not for the 0.4 ms pulse. It is, however, to be noted that even though the pulse times are the same, the dynamics of the system is different from the dynamics when simple pulse is used for activation. This is indicative of the fact that the

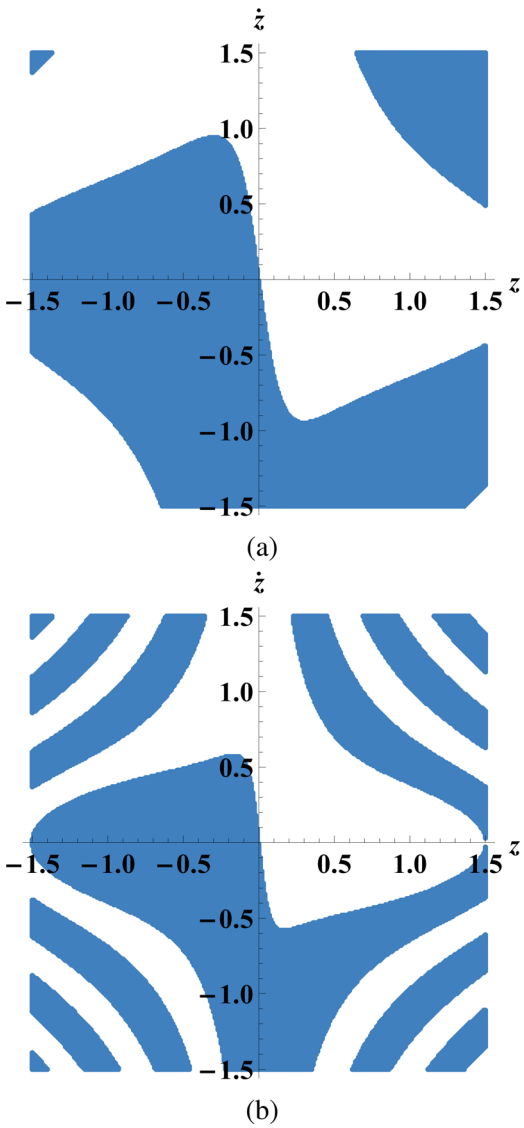

Fig. 8 Basins of attraction for the two stable configurations of the system buckled in its first mode when the load is (*a*) 1% and (*b*) 5% greater than the critical load. The mass of the actuator is 1.5 times the nominal value used in Fig. 5, and all other parameters are the same. Note that the blue areas represent the basin of attraction for the stable point (−1,0), and the white area represents the basin of attraction for the stable point (1,0).

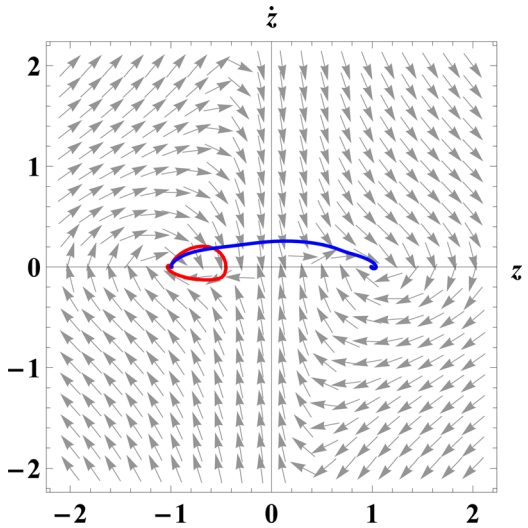

Fig. 9 Response of the system when actuated by a simple pulse input (5 mW) for 0.4 ms (red) and 0.8 ms (blue). The system is initially at the state (−1,0). It switches to the other stable state for the pulse of width 0.8 ms, but not for the pulse width of 0.4 ms.

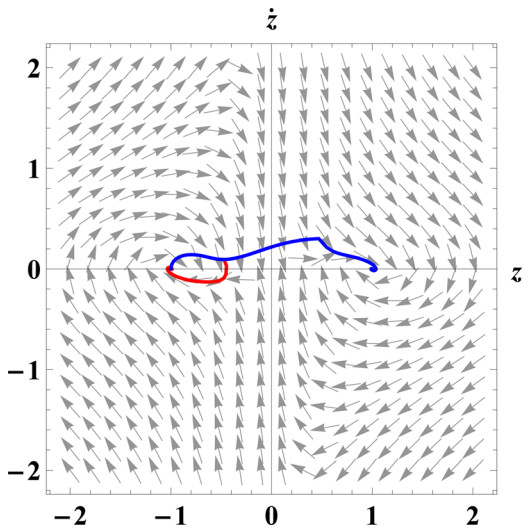

Fig. 10 Response of the system when actuated by a half-sine pulse input (5 mW) for 0.4 ms (red) and 0.8 ms (blue). The system is initially at the state (−1,0). It switches to the other stable state for the pulse of width 0.8 ms but not for the pulse of width 0.4 ms.

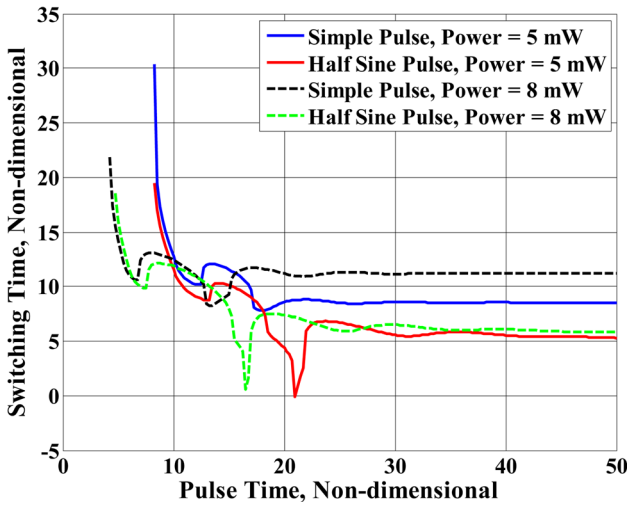

Fig. 11 Relationship between switching times and pulse widths for a simple pulse input and a half-sine wave input for two different pulse amplitudes when the axial load is 0.5% higher than the critical load of the beam. The pulse amplitudes are designed such that both of the inputs are of equal energy. The switching time is defined to be the time taken by the system to settle in the stable state (1,0), starting from the (−1,0) configuration, after the removal of the pulse.

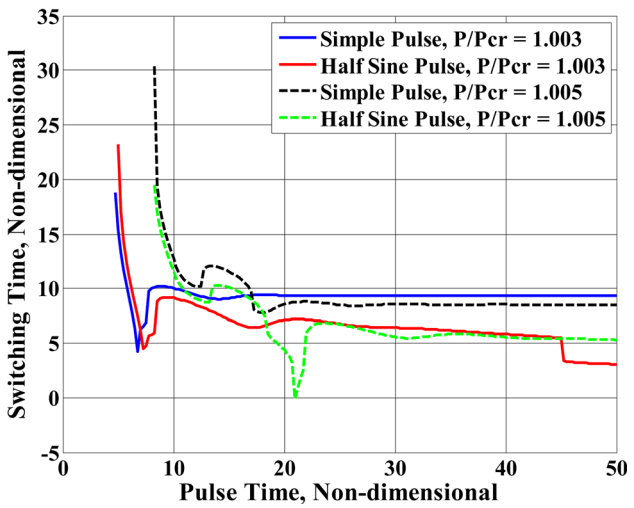

Fig. 12 Relationship between switching times and pulse widths for a simple pulse input and a half-sine wave input for two different values of critical load at the same excitation level (5 mW). The pulse amplitude are such that both the inputs are of equal energy. The switching time is defined here to be the time taken by the system to settle in the stable state (1,0), starting from the (−1,0) configuration, after the removal of the pulse.

switching dynamics is a function not only of pulse duration and amplitude but of the pulse profile itself.

To compare the effectiveness of various pulse profiles in optical switching, two test cases are analyzed, namely, the simple pulse and the half-sine wave pulse noted above. Figure 11 highlights the relationship between (nondimensional) pulse widths and (nondimensional) switching times, as measured after the pulse has been removed, for each actuation profile for two different optical power levels and an axial load that is 0.5% higher than the critical load. Note that the pulse widths are kept constant here, and the amplitudes of the pulses have been adjusted so that both pulses are of equal energy. The dashed lines correspond to the same energy level, as do the solid lines. It can be seen that the behavior is qualitatively invariant, but the pulse with a higher power has a reduced switching time for the same actuation time. In addition, it must also be noted that the settling times initially decrease and then increase as more energy is supplied to the system. This is attributable to the fact that the system can switch multiple times or oscillate excessively about a single stable position at higher energies. Accordingly, both the force and the duration of the force become critical in the design of optically-actuated bistable systems. Note that as the pulse width is increased, the system may possess very rich dynamic behaviors; however, in order to preserve the optimal switching behavior, the analysis has been limited to the pulse times shown in Fig. 11.

Figure 12 highlights the relationship between (nondimensional) pulse widths and (nondimensional) switching times, as measured after the pulse has been removed, for each actuation profile for two different values of compressive axial load. Note that the pulse

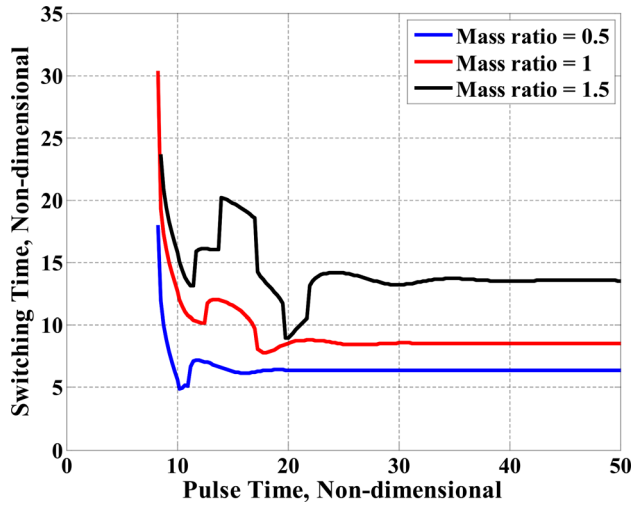

Fig. 13 Relationship between switching times and pulse widths for a simple pulse input for different values of the actuator mass (note that in this figure, mass ratio is the ratio of the mass of the actuator to the nominal value of the actuator mass) when the axial load is 0.5% higher than the critical load of the beam at the same excitation level (5 mW). The switching time is defined to be the time taken by the system to settle in the stable state (1,0), starting from the (−1,0) configuration, after the removal of the pulse.

widths were kept constant here and the amplitudes of the pulses have been adjusted so that both pulses are of equal energy. The solid lines and the dashed lines represent cases when the axial load is higher than the critical load by 0.3% and 0.5%, respectively. The dashed lines both correspond to the same energy level, as do the solid lines. As evident, for a constant energy pulse, there exists regions where the switching times associated with simple pulse inputs are smaller than those recovered with half-sine inputs and vice versa. As the axial load increases, these trajectories remain qualitatively alike but shift towards the right. This results in increased minimum actuation times and increased switching times.

Figure 13 shows the relationship between the (nondimensional) pulse widths and the (nondimensional) switching times for a simple pulse input for different values of the actuator mass (note that for ease of representation, a nondimensional term, mass ratio has been introduced. It is the ratio of the actuator mass considered to the nominal value of the actuator mass defined in Fig. 5), for an axial load that is 0.5% higher than the critical load. It can be seen that as the actuator mass increases, the system with a higher actuation mass has higher switching times for the same actuation time. Additionally, it is also notable that the minimum actuation time required for switching also increases with the actuator mass.

By extrapolating the methodologies detailed herein, the dynamics of the beam undergoing buckling in higher modes can be investigated. Preliminary analysis reveals that for loads comparatively higher than the critical buckling load, the system can exhibit rather complex dynamic behaviors. The onset of this complex behavior appears to have a nontrivial dependence on multiple system parameters, including damping and actuator mass, and, thus, will be addressed in a separate study.

4 Conclusions and Future Directions

In conclusion, this work considered the modeling and analysis of the post-buckled dynamics of a representative, bistable MEMS device optically-actuated by an external laser pulse. Through the use of forward-time numerical simulation, the impact of various system and excitation parameters, including applied axial load and optical actuation profile, on the transient behavior (switching times) of the representative device have been investigated. The methodologies and results presented herein should provide for a refined predictive design capability for small-scale bistable devices. It is important to note that the efforts described here are still in their infancy. Ongoing work is aimed at incorporating refined modal approximations, experimentally verifying predicted behaviors, and extending the predictions to device-specific applications.

Acknowledgment

The authors would like to thank Professors Arvind Raman, Charles Krousgrill, and Anil Bajaj of the School of Mechanical Engineering at Purdue University for their valuable inputs to this work. A preliminary version of this work initially appeared at the ASME 2010 International Design Engineering Technical Conferences and Computers and Information in Engineering Conference, 4th International Conference on Micro- and Nanosystems [21].

References

[1] Malevanets, A., and Kapral, R., 1996, "Links, Knots, and Knotted Labyrinths in Bistable Systems," Phys. Rev. Lett., **77**(4), pp. 767–770.
[2] Longtin, A., Bulsara, A., Pierson, D., and Moss, F., 1994, "Bistability and the Dynamics of Periodically Forced Sensory Neurons," Biol. Cybern., **70**(6), pp. 569–578.
[3] Emam, S., 2002, "A Theoretical and Experimental Study of Nonlinear Dynamics of Buckled Beams," Ph.D. thesis, Virginia Polytechnic Institute and State University, Blacksburg, VA.
[4] Chen, J.-S., and Liao, C.-Y., 2005, "Experiment and Analysis on the Free Dynamics of a Shallow Arch After an Impact Load at the End," J. Appl. Mech., **72**(1), pp. 54–61.
[5] Yabuno, H., and Tsumoto, K., 2007, "Experimental Investigation of a Buckled Beam Under High-Frequency Excitation," Arch. Appl. Mech., **77**(5), pp. 339–351.
[6] Latorre, L., Kim, J., Lee, J., de Guzman, P., Lee, H., and Nouet, P., 2002, "Electrostatic Actuation of Microscale Liquid-Metal Droplets," J. Microelectromech. Syst., **11**(4), pp. 302–308.
[7] Capanu, M., Boyd, J., IV, and Hesketh, P., 2000, "Design, Fabrication, and Testing of a Bistable Electromagnetically Actuated Microvalve," J. Microelectromech. Syst., **9**(2), pp. 181–189.
[8] Qin, J., 2003, "An Electrothermally Actuated Bistable MEMS Relay for Power Applications," Ph.D. thesis, Massachusetts Institute of Technology, Cambridge, MA.
[9] Saif, M., 2000, "On a Tunable Bistable MEMS - Theory and Experiment," J. Microelectromech. Syst., **9**(2), pp. 157–170.
[10] Sulfridge, M., Saif, T., Miller, N., and O'Hara, K., 2002, "Optical Actuation of a Bistable MEMS," J. Microelectromech. Syst., **11**(5), pp. 574–583.
[11] Sulfridge, M., Saif, T., Miller, N., and Meinhart, M., 2004, "Nonlinear Dynamic Study of a Bistable MEMS: Model and Experiment," J. Microelectromech. Syst., **13**(5), pp. 725–731.
[12] Krylov, S., Ilic, B. R., Schreiber, D., Serentensky, S., and Craighead, H., 2008, "The Pull-In Behavior of Electrostatically Actuated Bistable Microstructures," J. Micromech. Microeng., **18**(5), 055026.
[13] Krylov, S., and Dick, N., 2009, "Pull-In Dynamics of Electrostatically Actuated Bistable Micro Beam," International Design Engineering Technical Conferences and Computers and Information in Engineering Conference, 3rd International Conference on Micro- and Nanosystems, Paper No. DETC2009-87236.
[14] Lacarbonara, W., and Yabuno, H., 2006, "Refined Models of Elastic Beams Undergoing Large In-Plane Motions: Theory and Experiment," Int. J. Solids Struct., **43**(17), pp. 5066–5084.
[15] Luongo, A., Rega, G., and Vestroni, F., 2009, "On Nonlinear Dynamics of Planar Shear Indeformable Beams," J. Appl. Mech., **53**(3), pp. 619–624.
[16] Timoshenko, S., and Gere, J., 1961, *Theory of Elastic Stability*, 2nd ed., McGraw-Hill, New York.
[17] Zalalutdinov, M., Olkhovets, A., Zehnder, A., Ilic, B., Czaplewski, D., Craighead, H. G., and Parpia, J. M., 2001, "Optically Pumped Parametric Amplification for Micromechanical Oscillators," Appl. Phys. Lett., **78**(20), pp. 3142–3144.
[18] Aubin, K., Zalalutdinov, M., Alan, T., Reichenbach, R., Rand, R., Zehnder, A., Parpia, J., and Craighead, H., 2004, "Limit Cycle Oscillations in CW Laser-Driven NEMS," J. Microelectromech. Syst., **13**(6), pp. 1018–1026.
[19] Sulfridge, M., Saif, T., Miller, N., and O'Hara, K., 2001, "Actuation of MEMS by Light: An Optical Actuator," 2001 ASME International Mechanical Engineering Congress and Exposition, Paper No. IMECE2001/MEMS-23816.
[20] Cazottes, P., Fernandes, A., Pouget, J., and Hafez, M., 2009, "Bistable Buckled Beam: Modeling of Actuating Force and Experimental Validations," J. Mech. Des., **131**(10), 101001.
[21] Kumar, V., and Rhoads, J. F., 2010, "Modeling and Analysis of an Optically-Actuated Bistable MEMS Device," 2010 International Design Engineering Technical Conferences and Computers and Information in Engineering Conference, 4th International Conference on Micro- and Nanosystems, Paper No. DETC2010-29040.